TECHNICAL MEMORANDUM

549

A 5-year 40-km resolution global climatology of super-refraction for ground-based radar meteorology

Philippe Lopez

Research Department

January 2008

European Centre for Medium-Range Weather Forecasts
Europäisches Zentrum für mittelfristige Wettervorhersage
Centre européen pour les prévisions météorologiques à moyen terme

Series: ECMWF Technical Memoranda

A full list of ECMWF Publications can be found on our web site under:
http://www.ecmwf.int/publications/

Contact: library@ecmwf.int

European Centre for Medium-Range Weather Forecasts
Shinfield Park, Reading, RG2 9AX, England

Abstract

The propagation of electromagnetic beams emitted from ground-based meteorological radars is determined by the stratification of the atmosphere. In extreme super-refractive situations characterized by strong temperature inversions or strong vertical gradients of moisture, the radar beam can be deflected towards the ground (ducting or trapping). This often results in spurious returned echoes and mis-interpretation of radar images such as erroneous precipitation detection. In this work, a 5-year global climatology of the frequency of super-refractive and ducting conditions and of trapping layer base height has been produced using refractivity computations from ECMWF temperature, moisture and pressure analyses at a 40-km horizontal resolution. The aim of this climatology is to better document how frequent such events are, which is prerequisite to fully benefit from radar data information for the multiple purposes of model validation, precipitation analysis and data assimilation. First, the main climatological features are summarized for the whole globe and a particular focus is then laid on Europe and the U.S.A., where extensive precipitation radar networks already exist. Finally, the sensitivity of ducting occurrence to radar height is assessed by initiating refractivity vertical gradient computations from either the lowest or the second lowest model level.

1 Introduction

Ground-based meteorological radars are being extensively used to obtain valuable information on the spatial distribution and time evolution of a wide range of atmospheric parameters, in particular hydrometeors and cloud fields (amounts, particle size distribution and shape) as well as wind. Electromagnetic pulses are emitted with a tilt about the horizontal plane that can vary between 0.5 and 90 degrees (vertically pointing), depending on the desired detection range and type of application. The propagation of electromagnetic radiation through the atmosphere at typical wavelengths used in radar meteorology (namely between 1 mm and 10 cm) is directly related to the spatial variations of refractivity, which is itself mainly a function of air temperature, pressure and humidity. In particular, vertical gradients of refractivity and thus the vertical stratification of the atmosphere determine the path followed by a radar beam. In certain meteorological conditions described below, low-tilt beams emitted from ground-based radar can become trapped and even be deflected towards the surface, leading to spurious backscattered signals and hence erroneous interpretation (e.g. false precipitation echo). This phenomenon is referred to as *anomalous propagation* (AP) and the layer inside which the beam moves downwards is called the *duct*.

The use of ground-based radar data is bound to increase in the future not only for model validation but also for the production of precipitation analyses (e.g. Mahfouf *et al.* 2007) as well as in data assimilation. In the latter context, it is hoped that radar data can improve the quality of initial conditions for numerical weather prediction (NWP) models through either nudging techniques (e.g. Macpherson 2001), diabatic initialization (e.g. Ducrocq *et al.* 2002) or more elaborate data assimilation procedures such as 4D-Var (e.g. Lopez and Bauer 2007) or Ensemble Kalmán Filter (Tong and Xue 2005). With horizontal resolution reaching 10 kilometers or less, the excellent sampling in both space and time of radar observations make them particularly appealing to constrain initial conditions of mesoscale models (e.g. Sun 2005). However, radar measurements can only be profitable if data affected by AP can be screened out prior to the desired application. AP contamination is sometimes filtered out through radar image processing techniques or Doppler signal analysis (when available and over land only), but the efficiency of these methods is far from 100%.

On a climatological standpoint, it is important to assess how often a given region of the globe is likely to experience conditions favourable to AP. For instance, such knowledge can be used by radar network developers to select optimal sites for new instruments. It can also help to identify regions where model verification, precipitation analysis and data assimilation based on radar data are likely to be unreliable because of frequent AP situations. In the literature, von Engeln and Teixeira (2004) proposed a 6-year global 1.5° resolution climatology of ducting events from the prospect of radio-occultation measurements from the spaceborne Global

Position System (GPS). In their study, only the first highest duct when looking downwards was considered and the rather coarse resolution used implied that only horizontally widespread ducts were included in the statistics. The goal of the present paper is to introduce a 5-year global climatology of AP events *from the viewpoint of ground-based radars* and derived from ECMWF operational analyses at roughly 40-km horizontal resolution, which should provide information on a much finer scale over individual regions such as Europe and the United States.

Section 2 defines the various refraction regimes and explains how ducts can be simply identified from temperature, humidity and pressure profiles. The ECMWF data used in this study are briefly described in section 3, while some remarks about the computation of refractivity vertical gradients are expressed in section 4. The main features of the global climatology of AP conditions are presented in section 5, which also includes a more detailed analysis of ducting occurrences over Europe and the U.S.A. where precipitation radar networks are already well developed. Then, the sensitivity of the climatological statistics to radar tower height is discussed in section 6. Summary and conclusions are given in section 7.

2 Definition of refraction regimes

The propagation of radar beams through the atmosphere is governed by Snell's law that is by the spatial variations of the index of refraction, n, or, equivalently, to those of refractivity, $N = (n-1) \times 10^6$ (n is close to unity for the air). N can be computed from temperature, T (in K), partial pressure of water vapour, e (in Pa), and atmospheric pressure, p (in Pa), using

$$N = \frac{0.776p}{T} + \frac{3730e}{T^2} \tag{1}$$

Typical values of N range between 140 and 450. As vertical variations of temperature, moisture and pressure dominate over horizontal ones, the propagation of radar beams mainly depends on the vertical gradient of refractivity. The effect of the Earth's curvature (radius R) at an altitude z can be accounted for by considering a modified refractivity, M, defined as

$$M = N + \frac{z \times 10^6}{R} \tag{2}$$

Ducting (or radar beam trapping) usually occurs for beams with small tilt angles (less than 1°) above the local horizon when $\partial M/\partial z < 0$ or in other words when $\partial N/\partial z \leq -10^6/R \approx -0.157$ m^{-1}, assuming R can be approximated by the Earth's radius throughout the troposhere. In fact, four different propagation regimes are usually considered:

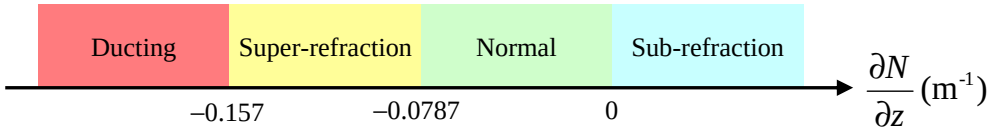

From Eq. (1) one can deduce that conditions favourable to the super-refractive and ducting regimes must involve layers exhibiting either an increase of temperature or a sharp decrease of moisture with height. As $\partial N/\partial z$ gets lower than -0.157 m^{-1}, the electromagnetic beam gets deflected towards the surface and spurious ground echoes (or *clutters*) are returned to the radar. Figure 1 gives an illustration of the different propagation regimes.

One should note that the *trapping layer* (TL) is defined as the layer inside which $\partial M/\partial z$ remains negative.

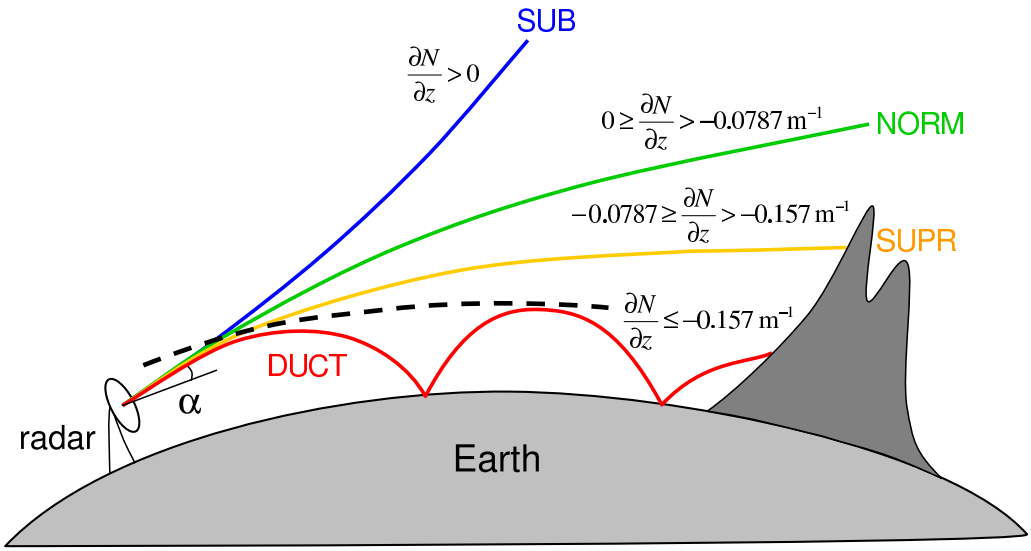

FIGURE 1: The different propagation regimes of a ground-based radar beam emitted with a small tilt angle, α, above the horizontal: subrefraction (blue), normal refraction (green), super-refraction (orange) and ducting (red). The corresponding values of refractivity gradient, $\partial N/\partial z$, are indicated above each beam path. The dashed line indicates the top of the duct.

This layer is always embedded inside the *duct* which extends, by definition, from the TL top down to either the surface or the level at which M becomes equal to the value at TL top. Depending on the shape of the modified refractivity profile, three types of ducts can be identified as sketched in Fig2: surface duct in panel (a), S-shaped surface duct in panel (b) and elevated duct in panel (c).

The most common meteorological situations involving super-refractivity or, worse, ducting are:

- temperature inversion due to nocturnal radiative cooling inside the Planetary Boundary Layer (PBL) over land,
- temperature inversion over a moist PBL, due to anticyclonic subsidence in the tradewind region,
- dry air advection over sea or wet land,
- low-level moist and cool air advection from the sea,
- outflow of low-level moist and cold air from thunderstorms.

In practice, the ducts that affect ground-based radars are always confined to the lowest 3000 m of the troposphere. One should note that AP ground clutters can also be observed in the super-refractive regime in the absence of ducting when the radar beam is refracted downwards and impinges on surrounding orography (*beam blocking*), as shown in Fig. 1 (yellow path).

To efficiently deviate a radar beam towards the surface, a TL must have a minimum depth, D_{min}, which is expectedly a function of the magnitude of the vertical refractivity gradient but also of the radar signal wavelength, λ. The simplified formula proposed by Turton *et al.* (1988) leads to the expression

$$D_{min} = \left\{ C\lambda \left(-\frac{\partial N}{\partial z} \right)^{-\frac{1}{2}} \right\}^{\frac{2}{3}} \tag{3}$$

where λ and D_{min} are in meters and C =400 (resp. 263) for surface (resp. elevated) ducts. For a wavelength of 10 cm, which is typical of precipitation radars and which corresponds to the upper end of the wavelength

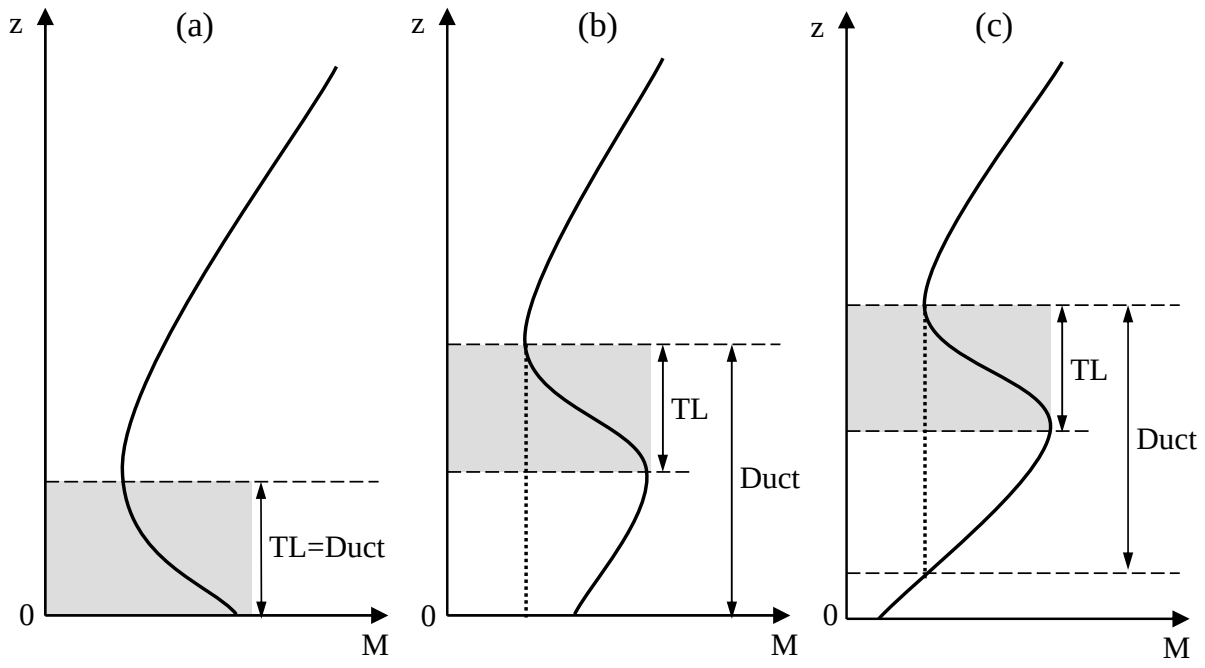

FIGURE 2: Duct types as a function of the shape of the modified refractivity (M) vertical profile: (a) surface duct, (b) S-shaped surface duct, and (c) elevated duct. Grey shading identifies the trapping layer (TL).

range used in radar meteorology, the minimum depth required for a ducting layer to deviate most of the radar beam is approximately equal to 22 m (resp. 16 m) for a surface (resp. elevated) duct. More generally, Eq. (3) shows that D_{min} becomes smaller when wavelength is reduced as well as when $\partial N/\partial z$ becomes more negative (increased duct intensity). This has some implications for the efficiency of ducts detection from model outputs, as explained in section 4.

3 ECMWF operational analyses

The climatological statistics are computed from ECMWF operational analyses for the period between 1 December 2000 and 30 November 2005. ECMWF operational analyses are produced using a four-dimensional variational (4D-Var) data assimilation system, as described in Courtier et al. (1994). All analysis fields are retrieved on the original T511 reduced Gaussian grid, which corresponds to a quasi-uniform horizontal resolution of about 40 km over the globe. Temperature and moisture profiles are extracted on the operational 60 vertical levels (hybrid η-coordinate). As an illustration of the model vertical resolution, the thickness of each model layer up to a 10-km height is displayed in Fig. 3. Note that the actual height of each model level may vary slightly among model grid points due to horizontal variations of virtual temperature and surface pressure. The current operational T799 L91 configuration could not be used in this study because these enhanced resolutions were implemented less than two years ago, a period of time deemed too short for building a reasonable climatology. As far as timeliness is concerned, analyses valid at 0000, 0600, 1200 and 1800 UTC are used in order to somewhat crudely sample the diurnal cycle.

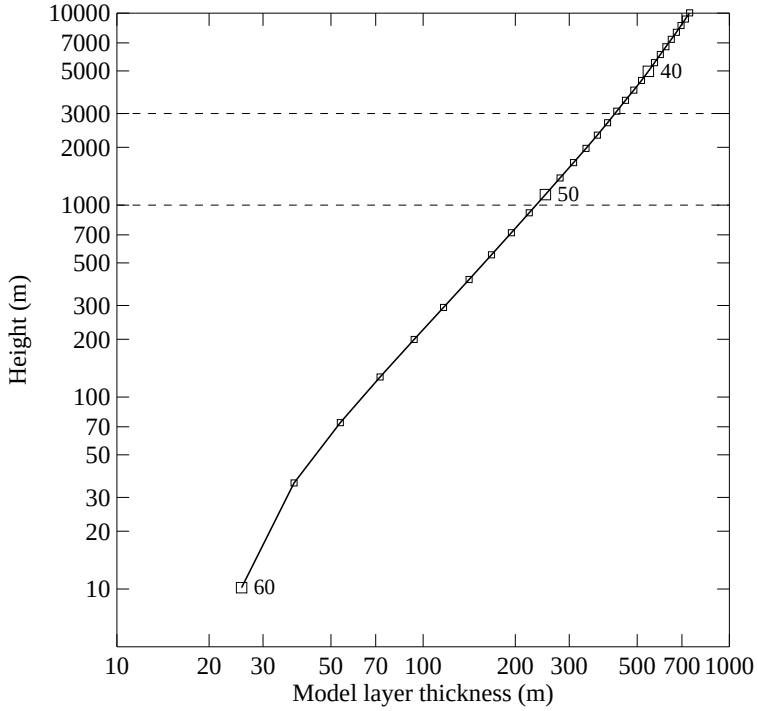

FIGURE 3: Model layer thickness as a function of bottom layer height. Units on both logarithmic axes are in meters. Model levels 40, 50 and 60 are explicitly labelled.

4 Refractivity gradient calculations and statistics

Refractivity is computed from Eq. (1) and the minimum vertical gradient is estimated over all model layers starting from the lowest model level (about 10 m height) up to a height of 3000 m. This maximum height limitation is imposed as a result of the degradation of model vertical resolution with height, as illustrated in Fig. 3, and because most ducts affecting ground-based radars are found below this level. It is worth noting that such restriction was also applied in Von Engeln and Teixeira (2004). On the other hand, the gradient computations are started at the lowest model level and not directly from the surface to account for the fact that most meteorological radars are installed at least 10 m above the ground (towers). In other respects, since Eq. (3) indicated a minimum depth, D_{min}, of about 20 m, Fig. 3 suggests that most TLs that lie within a few tens of meters above the surface are expected to be properly identified from analysis fields while only the deepest elevated TLs can be resolved, especially above 1000 m. At the same time, it also means that any TL detected from model analyses is deep enough to fully refract the radar beam downwards.

In this study, statistics are calculated not only for ducting but also for super-refractive situations. Super-refraction (resp. ducting) is assumed to occur whenever the minimum value of $\partial N/\partial z$ is lower than -0.0787 m^{-1} (resp. $-0.157\ \mathrm{m}^{-1}$). Note that in the following all occurrences of ducting events are also counted as super-refractive cases. For each model grid point, statistics will be presented in terms of the frequency of occurrence of super-refractive and ducting events but also in terms of the bottom height of the first TL encountered from the surface, h_b.

5 Results

5.1 Global climatological features

Maps of the global seasonal mean frequencies of occurrence of super-refractive and ducting conditions are displayed in Fig. 4 and Fig. 5 respectively. Seasonal mean TL base heights, $\overline{h_b}$, are shown in Fig. 6. One should remember that TLs with a base above 3000 m above the surface are disregarded in this study. Also note that for the sake of brevity all four analyses times have been averaged to construct these global maps. Information about the diurnal variations of these statistics will be detailed in section 5.2 which focuses on Europe and the U.S.A..

Some yearlong features can be identified over sea in Fig. 4 and Fig. 5: the North Atlantic, North Pacific and, above all, Southern Oceans are seldom affected by super-refraction and ducting as a result of the ceaseless and intense storm activity and the associated strong vertical mixing of the troposphere. In opposition, the tropical oceans are characterized by persistent super-refraction because of the combined effects of the trade-wind temperature inversion and of the strong evaporation from the sea surface (sharp upward decrease of moisture inside the PBL). In particular, the frequency of ducts is well above 50% over the colder waters east of the subtropical deserts (South Africa, South America, Mexico, West Africa and Australia) and Fig. 6 shows that $\overline{h_b}$ rises westards from less than 200 m close to the coast up to 1200 m in the middle of each ocean basin, following the level of the temperature inversion. In the trade-wind regions, the day-to-day fluctuations of h_b are generally small compared to $\overline{h_b}$ (not shown). The Arabian Sea, the Red Sea and the Persian Gulf, where intense surface evaporation into subsident dry air is commonly observed, also appear to be strongly affected by super-refraction and ducting all year round. A detailed case-study of the mechanisms involved in the formation of intense ducts in the Persian Gulf can be found in Atkinson and Zhu (2005).

Over land regions, super-refractive and ducting events are generally less frequent than over tropical oceans, with stronger seasonal variability. Super-refractivity over tropical continents remains pronounced over moist regions, including equatorial Africa, the Amazonian Basin, and South East Asia. At mid-latitudes, the south-eastern U.S.A. are the most affected especially during summer, because of the strong moisture supply from the surface due to heavy precipitation and due to the presence of the Mississipi, Missouri, and Ohio rivers. Greenland, Siberia and Antarctica are exposed to very frequent super-refractive and ducting conditions in the wintertime, which are associated with low-level temperature inversions during the polar night. Elsewhere in the extra-tropics, the frequency of occurrence of super-refraction and ducting is often lower than 50% and 20% respectively. In addition, Fig. 6 confirms that $\overline{h_b}$ over land usually lies below 70 m, as a result of the strong influence of surface processes (low-level temperature inversion, surface latent heat flux) on refractivity gradients. Higher TL base heights are found in regions of intense convection, especially over the Sahel and India during the summer monsoon, and over the southeastern U.S.A and Argentina all year round.

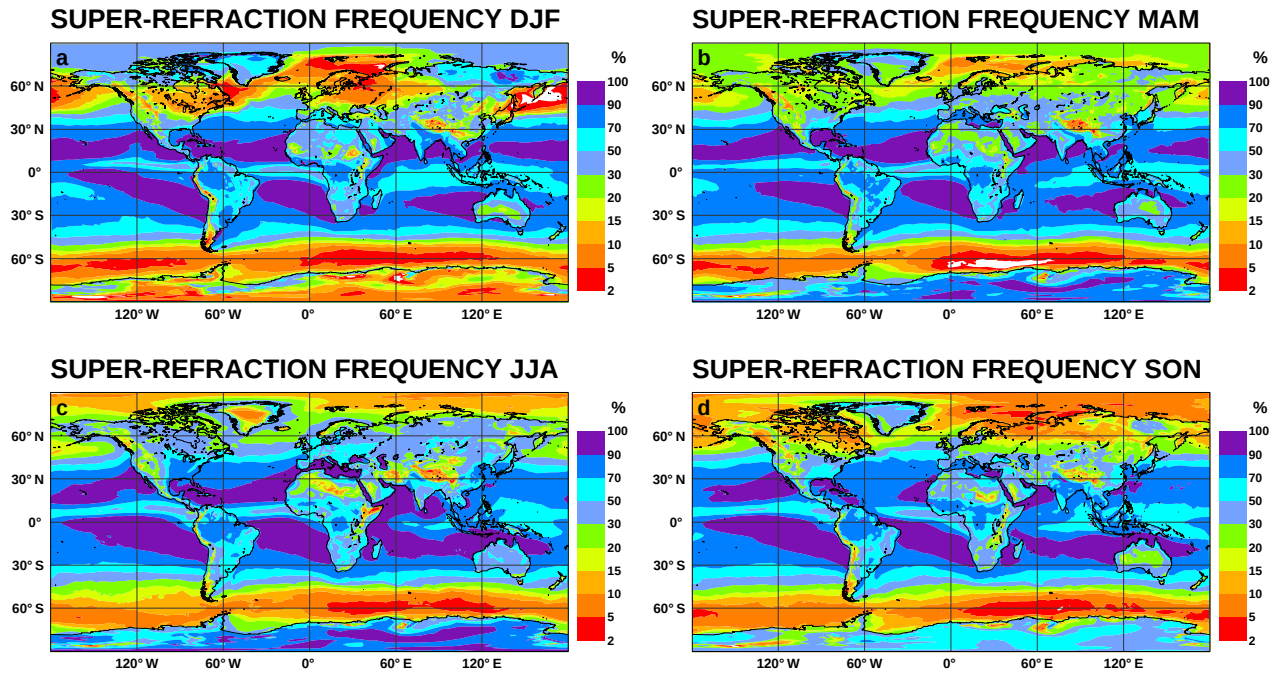

FIGURE 4: Global seasonal mean frequency (%) of super-refractive conditions for (a) winter, (b) spring, (c) summer and (d) autumn. The averaging has been performed over analyses times 0000, 0600, 1200 and 1800 UTC.

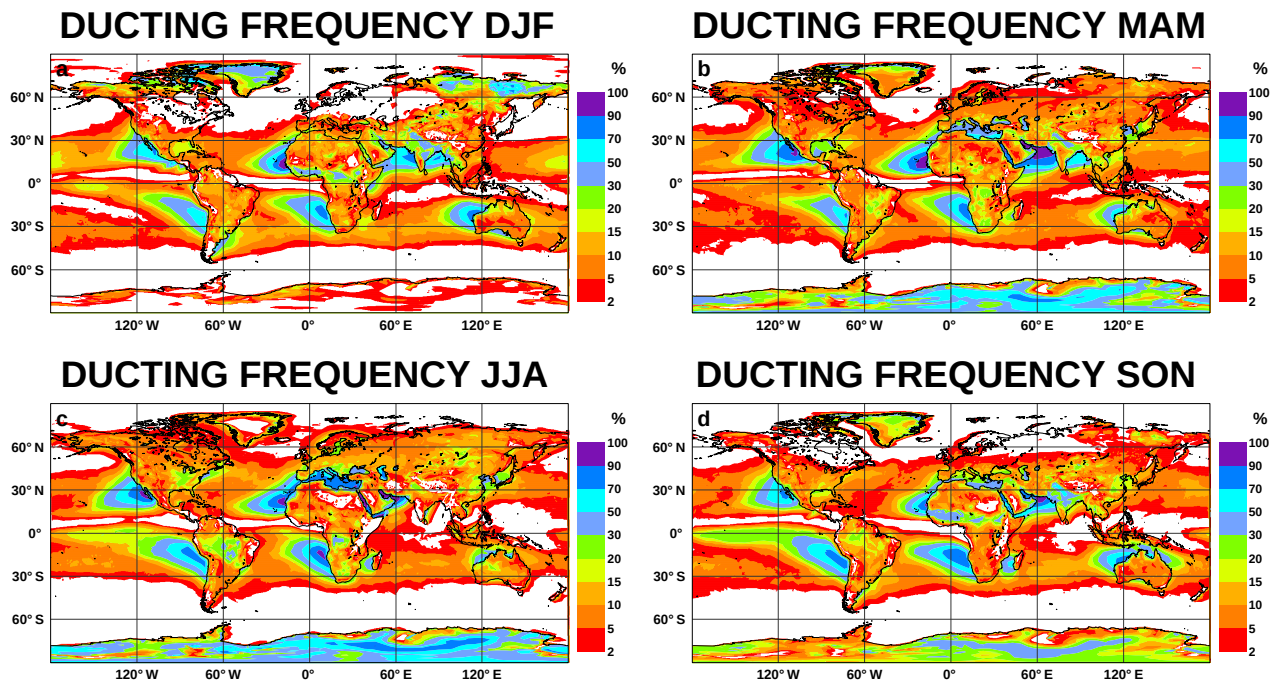

FIGURE 5: Same as in Fig. 4, but for the mean frequency of ducting conditions.

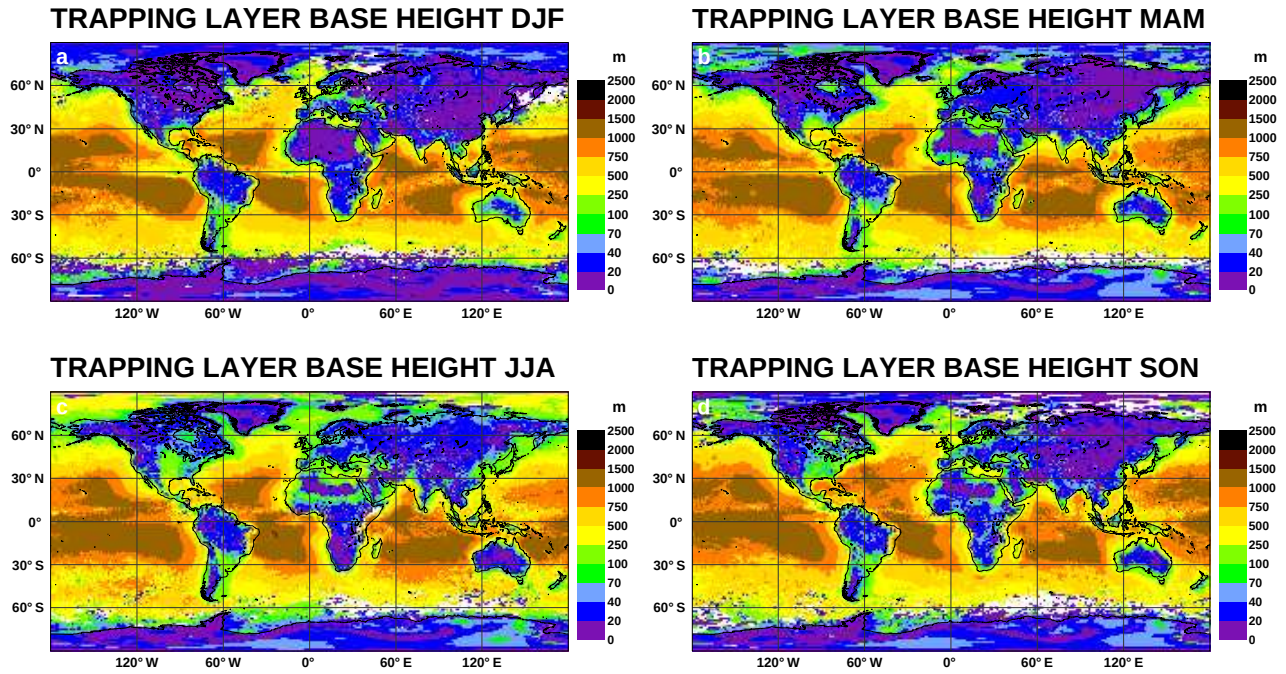

FIGURE 6: Same as in Fig. 4, but for mean duct base height (m). White shading corresponds to regions without ducting.

5.2 Regional climatological features

Climatological statistics for Europe and the U.S.A. will now be presented in more details because these two regions already benefi t from a widespread network of ground-based precipitation radars that are used for the purpose of operational weather and hydrological forecasting. Over the U.S.A., the network of more than 150 NEXt generation RADars (NEXRAD) is used by NCEP to produce almost real-time hourly precipitation analyses (Lin and Mitchell 2005). Similarly in Europe, the Operational Programme for the Exchange of weather RAdar information (OPERA) is currently aiming at unifying the data obtained from about 150 radar sites available in more than twenty countries (Huuskonen 2006).

5.2.1 Europe

Ducting occurrence

Figure 7-10 display the diurnal cycle of ducting occurrence for each season over Europe.

Over the entire domain, ducting frequencies are generally minimum in winter and maximum in summer, with intermediate values in spring and autumn. In all seasons, over land, ducts are almost completely absent at 1200 UTC, as seen in panels (c) of Fig. 7-10. Indeed, the development of sharp low-level refractivity gradients in daytime is hindered by the intense tropospheric mixing associated with the strong solar heating and convective activity from spring to autumn, and by the relative weakness of water vapour partial pressure and storminess in wintertime. From early night to early morning (panels (a) and (b) of Fig. 7-10), ducts are more likely to appear as a result of the nocturnal surface cooling and increased stability which favour the build-up

of low-level temperature inversion and sharper negative vertical gradients of moisture. Over Central Europe, occurrences of ducts are more frequent at 1800 UTC than at night. During summer nights, Southern Spain, the Balkans but above all most of Italy exhibit rather high ducting frequencies (above 30%). Throughout the year, the Po Valley turns out to be the European region with the strongest probability of ducting events, in agreement with the local climatological study of anomalous propagation events proposed by Fornaserio *et al.* (2006). On the other hand, Scandinavia and the British Isles seem only marginally affected by ducting, mainly in spring and summer.

The seasonal cycle is very pronounced over the Mediterranean Sea with maximum duct frequencies nearing 100% in summer but falling well below 15% in winter, with little diurnal variations on average. Similar seasonal variations can be found over the Baltic sea, the Gulf of Biscay and the Black Sea, with a weaker amplitude though, while the North Atlantic Ocean is virtually duct-free.

Mean trapping layer base heights

As far as mean trapping base heights are concerned, Figure 11-14 indicate that values of $\overline{h_b}$ at 0000 and 1800 UTC are below 70 m over the entire European continent. At 0600 UTC, earlier sunrise times over Eastern Europe imply that morning surface heating (and thus turbulence) is already active, leading to a rise of TL base up to a height of 100 to 250 m. All year round, $\overline{h_b}$ at 1200 UTC (panels (c)) is usually well above 100 m over land, especially during the warm season, although these values should be taken with some caution given the very low frequency of ducting occurrence in daytime (Fig. 7-10). Over sea, $\overline{h_b}$ exceeds 100 m in all seasons, except over the Baltic Sea, the Adriatic Sea and the Black Sea in spring, as a consequence of the cold sea surface temperatures favouring persistent near-surface temperature inversions.

5.2.2 U.S.A.

Ducting occurrence

Figure 15-18 display the diurnal cycle of ducting occurrence for each season over the U.S.A.. One should note that due to longitude lag, times 0000, 0600, 1200 and 1800 UTC roughly correspond to local late afternoon, midnight, early morning and midday, respectively.

In winter (Fig. 15), the northern states remain virtually duct free all day long as a result of the low moisture content in the prevailing cold air masses. Further south, ducting frequencies remain below 20%, except over southern California and Arizona at night (up to 55% locally in panels (b) and (c)) and over Florida in late afternoon (panel (a)). The formation of nighttime ducts over the Southwest can be explained by the combination of prevailing stable conditions and low-level moisture advection from the nearby ocean. Figure 15d shows that ducts disappear almost completely in daytime (due to increased turbulence in the PBL) throughout the country, except on the West Coast. In fact, this widespread absence of ducts in daytime is found in other seasons as well (see panel (d) of Fig. 15-18). The same phenomenon also affects the Rocky Mountains in the late afternoon (local time) as seen in panels (a) of Fig. 15-18. From spring to autumn, each time of the day exhibit very similar patterns, that is duct frequencies reaching 60% over California and Arizona at night (panels (b) and (c)) for the reasons presented above, as well as along the Mississipi Valley and the East Coast, especially in the evening (panel (a)). Over the latter regions, heavy precipitation during the warm season peaks in the afternoon (e.g. Ahijevych *et al.* 2003), which favours the development of surface evaporation ducts in the evening. Evaporation from the Mississipi, Missouri and Ohio rivers further contributes to the formation of ducts. Over the tops of the Rocky mountains and the Appalachians, ducts are generally much less likely to occur than in surrounding valleys and plains. Over the Appalachians, for instance, this effect is very clearly in panels (a).

Over sea, extreme super-refractive conditions prevail off the coast of California and particularly around the

peninsula of Baja California, all day and all year round. Indeed, the presence of subsident dry air at mid-levels combines with the intense evaporation from the sea to create sharp negative gradients of moisture at lower levels and thus strong persistent surface ducts. Furthermore, the diabatic heating associated with large-scale subsidence above the relatively cold waters produces a low-level temperature inversion which make ducts even stronger. Over the Gulf of Mexico, except near Florida, ducting frequency reaches 30% in spring (Fig. 16) and is minimum in summer (less than 15%), with little diurnal variations in all seasons. More frequent vertically unstable conditions and the absence of strong positive air-sea temperature differences can account for these lower levels of ducting activity compared to the Pacific waters. West of the coast of Florida, duct frequencies in winter and spring are often higher than over the rest of the Gulf of Mexico, with a more pronounced diurnal cycle as well. Over the Great Lakes (especially Michigan), the mean ducting frequency is often higher than over surrounding land areas (surface evaporation ducts), except in winter when ducts are virtually non-existent.

Mean trapping layer base heights

In terms of mean TL base heights, Fig. 19-22 show that $\overline{h_b}$ is lower than 70 m over most of the U.S.A. at night (panels (b) and (c)) in all seasons, except around the Gulf of Mexico from spring to autumn ($\overline{h_b} \approx$70-500 m) as well as in the lee of the Rocky Mountains in summer ($\overline{h_b} \approx$70-250 m). Similar conclusions can be drawn for the late afternoon (panels (a)), except over the Rocky Mountains where ducts are absent and over the Pacific coastal fringe where $\overline{h_b}$ is usually above 250 m. On the other hand, panels (d) of Fig. 19-22 indicate that by midday from spring to autumn, the much fewer ducts east of the Rocky Mountains lie well above 250 m, with $\overline{h_b}$ exceeding 1000 m in the South (Texas, Florida) and over the eastern states in summer.

Over the Pacific coastal waters, $\overline{h_b}$ remains fairly constant throughout the day in all seasons, with values of about 150 m close to the coast, gradually increasing eastwards. Over the Gulf of Mexico, $\overline{h_b}$ rises away from the coast starting from about 250 m (a little less, close to Florida) up to 700 m (resp. 1000 m) in spring and summer (resp. autumn and winter). Similar remarks apply to the Atlantic waters, except that the values of $\overline{h_b}$ at the coast are well below 250 m, especially north of Cape Hatteras. These low values agree with those found from helicopter measurements close to the coast of Virginia by Babin (1996).

6 Influence of radar tower height on ducting occurrence statistics

As mentioned in section 4, the climatology thus far described (hereafter denoted CLIM10) was obtained by starting the calculations of the refractivity vertical gradient from the lowest model level (z_{min}), to account for the fact that most meteorological radars are installed at least 10 m above ground level (AGL). In fact, the height of the towers dedicated to these instruments can reach even greater heights. For instance, among the 154 NEXRAD radars in the U.S.A., a third or so are installed higher than 30 m AGL and more than 40% at a height around 20 m AGL. Since the steepest refractivity gradients over land are often found within the lowest 50 m of the troposphere, an alternative global climatology of super-refractive conditions was produced by starting the computations from the second lowest model level ($z_{min} \approx$35 m). This alternative climatology will be referred to as CLIM35 and is obviously expected to exhibit less frequent super-refractive and ducting events than CLIM10 whenever strong refractivity gradients are present below $z =$35 m.

Over sea, the reduction in these frequencies from CLIM10 to CLIM35 remains rather small (less than a few percents on average; not shown) because super-refraction is often associated with inversion layers that lie several hundred meters above the ocean surface (Fig. 6). Over land, in contrast, frequency differences are more pronounced. As an illustration, Tables 1 and 2 compare spatial averages of ducting frequencies for each season and time of the day over Europe and the U.S.A. (land only) between CLIM10 and CLIM35.

Europe	0000 UTC	0600 UTC	1200 UTC	1800 UTC
Winter	3.3	3.4	1.1	3.4
	2.0	**2.3**	**1.0**	**1.1**
Spring	9.6	8.4	0.3	12.8
	5.6	**6.8**	**0.2**	**2.8**
Summer	15.5	14.6	0.9	17.6
	10.4	**12.7**	**0.8**	**5.4**
Autumn	6.3	6.3	1.0	7.5
	3.8	**4.8**	**1.0**	**2.0**

TABLE 1: Spatially averaged frequencies of ducting occurrence (in %) over Europe (land only) at various times of the day and for each season from the two climatologies CLIM10 (normal font) and CLIM35 (bold font).

U.S.A.	0000 UTC	0600 UTC	1200 UTC	1800 UTC
Winter	5.9	7.3	6.6	1.7
	0.6	**3.3**	**4.0**	**1.7**
Spring	8.4	11.0	10.4	1.3
	1.2	**5.7**	**6.7**	**1.2**
Summer	12.8	14.2	15.7	2.3
	2.7	**8.7**	**10.9**	**2.1**
Autumn	10.4	11.5	10.9	2.1
	1.7	**5.8**	**6.9**	**2.0**

TABLE 2: Same as in Table 1, but for the U.S.A. (land only).

For both areas, the largest decrease (more than 10%) in frequencies occur in the summertime and in the evening (1800 UTC in Europe, 0000 UTC in the U.S.A.). This can be explained by the fact that temperature inversions are then confi ned to a very thin layer close to the surface, which makes the computations of refractivity gradients very sensitive to the value assigned to z_{min}. These shallow inversions associated with high occurrences of ducting (as seen in Fig. 9d and Fig. 17a) correspond to the very low TL base heights found in Fig. 13d over Europe and in Fig. 21a over the eastern half of the U.S.A.. On the other hand, ducting frequencies are less sensitive to z_{min} (2-5% drop only) during summer nights because, by then, inversion layers in those same regions have risen above 35 m, as indicated in Fig. 13a and Fig. 21b. Similar remarks apply to spring and autumn, with slighly weaker reductions though. In the winter season as well as during local daytime, the impact of z_{min} is small in absolute terms.

Locally, the summertime reduction of ducting occurrence when z_{min} is changed from 10 m to 35 m can reach very high values, as illustrated in Fig. 23. These two maps, valid for late afternoon over Europe and the U.S.A., show that in the Po Valley, the northern Balkans and the Mississipi Valley, installing a radar at a height of 35 m instead of 10 m above the ground can cut ducting probability by more than 40% (from 60% to 20%) over the whole summer season. This is very signifi cant, keeping in mind the disastrous effects of undetected anomalous propagation on the interpretation and potential usage of precipitation radar images.

7 Conclusions

A 5-year climatology of the frequency of atmospheric super-refraction and ducting occurrences and of trapping layer base height has been constructed by deriving refractivity gradients from ECMWF analyses at a 40-km resolution and using 60 levels in the vertical. It would be useful to repeat this work as soon as the volume of analyses available at T799 L91 resolution becomes large enough, since more levels in the vertical could improve the detection of ducts, especially away from the ground.

The purpose of this work was to provide a relatively high-resolution global database of AP that can be used for various applications of ground-based radar observations, such as validation of NWP outputs or even data assimilation. The statistics presented here might also be helpful to the GPS satellite radio-occultation community since the occurrence of ducting is known to degrade the accuracy of refractivity retrievals obtained from bending angle measurements.

It is thought that within a few years time the assimilation of precipitation radar observations could become feasible in ECMWF's 4D-Var system, with some potential benefi t for the quality of the analyses and subsequent forecasts. However, a prerequisite is that any radar data point which is contaminated by AP should be screened out prior to assimilation. In my experience, observations that have been supposedly quality controlled can still suffer from AP contamination, especially when those data are available in quasi-real time, with limited automatic sanity checks applied to them. A homemade screening procedure could consist of applying the type of computations described in section 2 to the model background state, prior to the assimilation.

Acknowledgements

Sean Healy, Marta Janisková and Martin Miller from ECMWF should be acknowlegded for their review of this paper.

References

Ahijevych, D. A., Carbone, R. E., and Davis, C. A. (2003). Regional-Scale Aspects of the Diurnal Precipitation Cycle. In *Proceedings of the 31st Conf. on Radar Meteorology, Presentation 5B.3, Amer. Meteor. Soc., Seattle, WA, U.S.A., August 2003*. Available at http://ams.confex.com/ams/32BC31R5C/techprogram/programexpanded_172.htm.

Atkinson, B. W. and Zhu, M. (2005). Radar-duct and boundary-layer characteristics over the area of The Gulf. *Q. J. R. Meteorol. Soc.*, 131:1923–1953.

Babin, S. M. (1995). Surface Duct Height Distributions for Wallops Island, Virginia. *J. Appl. Meteor.*, 35:86–93.

Courtier, P., Thépaut, J.-N., and Hollingsworth, A. (1994). A strategy for operational implementation of 4D-Var using an incremental approach. *Q. J. R. Meteorol. Soc.*, 120:1367–1388.

Ducrocq, V., Ricard, D., Lafore, J.-P., and Orain, F. (2002). Storm-scale numerical rainfall prediction for five precipitating events over France: On the importance of the initial humidity field. *Weather Forecast.*, 17:1236–1256.

Fornaserio, A., Alberoni, P. P., and Bech, J. (2006). Statistical analysis and modelling of weather radar beam propagation in the Po Valley (Italy). *Nat. Hazards Earth Syst. Sci.*, 6:303–314.

Huuskonen, A. (2006). EUMETNET OPERA: Operational Programme for the Exchange of Weather Radar Information. In *Proceedings of the 4th Conf. on Radar in Meteorology and Hydrology (READ), Barcelona, 18-22 September 2006*. Available at http://www.grahi.upc.edu/ERAD2006/index.php.

Lin, Y. and Mitchell, K. E. (2005). The NCEP Stage II/IV Hourly Precipitation Analyses: Development and Applications. In *Proceedings of the 19th AMS Conference on Hydrology, San Diego, CA (USA), 5–14 January 2005*.

Lopez, P. and Bauer, P. (2007). "1D+4D-Var" Assimilation of NCEP Stage IV Radar and Gauge Hourly Precipitation Data at ECMWF. *Mon. Weather Rev.*, 135:2506–2524.

Macpherson, B. (2001). Operational experience with assimilation of rainfall data in the Met.Office mesoscale model. *Meteorol. Atmos. Phys.*, 76:3–8.

Mahfouf, J.-F., Brasnett, B., and Gagnon, S. (2007). A Canadian Precipitation Analysis (CaPA) Project: Description and Preliminary Results. *Atmosphere-Ocean*, 45:1–17.

Sun, J. (2005). Initialization and Numerical Forecasting of a Supercell Storm Observed during STEPS. *Mon. Weather Rev.*, 133:793–813.

Tong, M. and Xue, M. (2005). Ensemble Kalman Filter Assimilation of Doppler Radar Data with a Compressible Nonhydrostatic Model: OSS Experiments. *Mon. Weather Rev.*, 133:1789–1807.

Turton, J. D., Bennetts, D. A., and Farmer, S. F. G. (1988). An introduction to radio ducting. *Meteor. Mag.*, 117:245–254.

von Engeln, A. and Teixeira, J. (2004). A Ducting Climatology derived from ECMWF Global Analysis. *J. Geophys. Res.*, 109. (D18), D18104, doi:10.1029/2003JD004380.

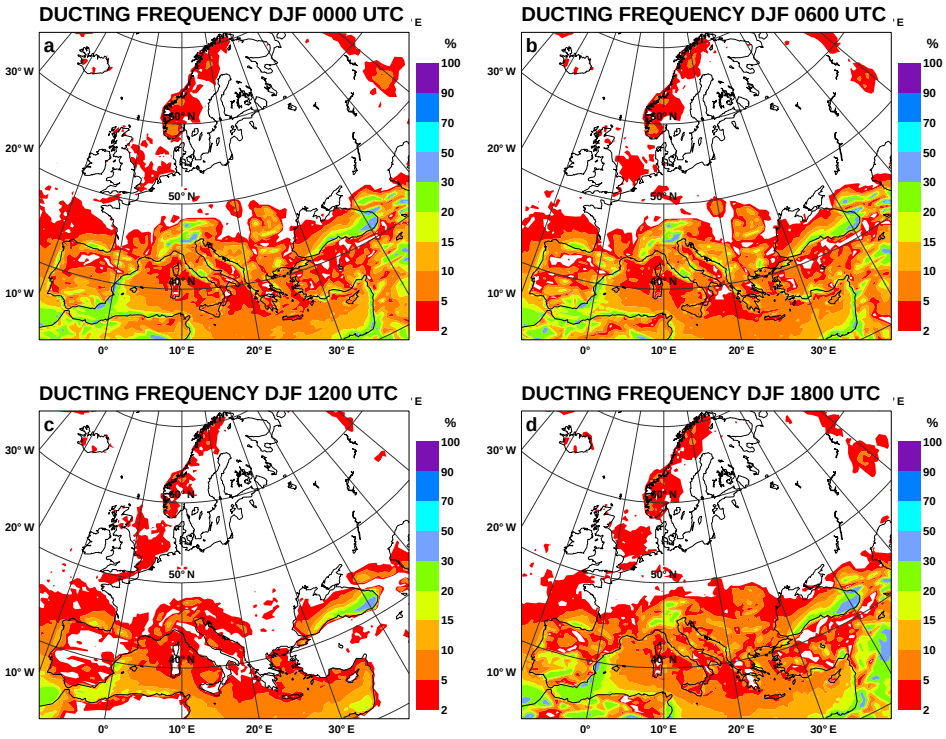

FIGURE 7: Mean winter frequency (%) of ducting conditions over Europe at (a) 0000, (b) 0600, (c) 1200 and (d) 1800 UTC.

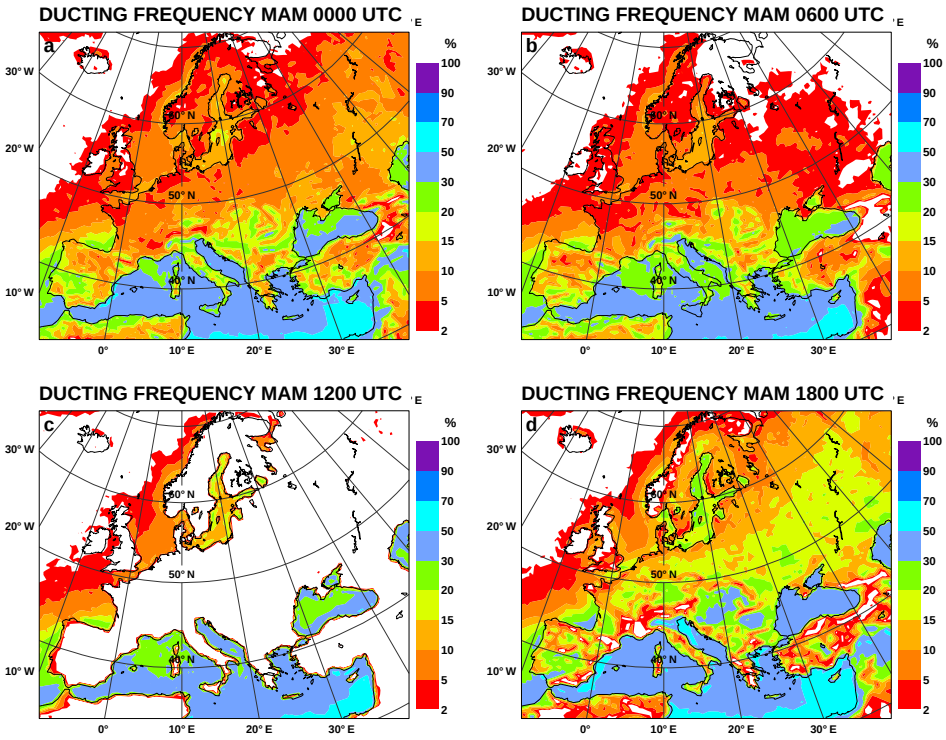

FIGURE 8: Same as in Fig. 7, but for spring.

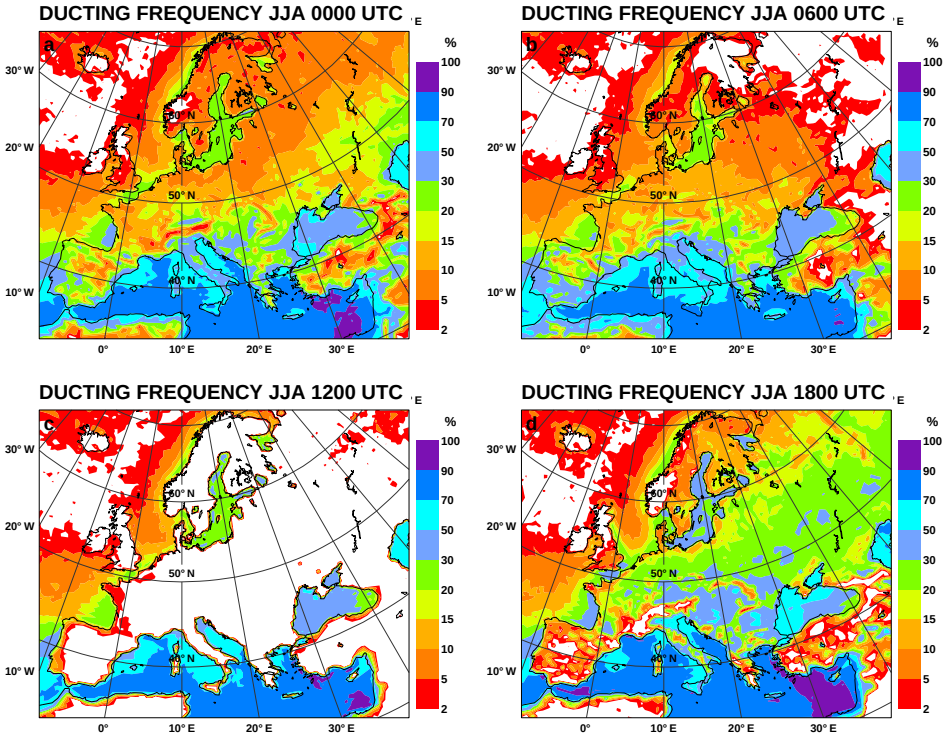

FIGURE 9: Same as in Fig. 7, but for summer.

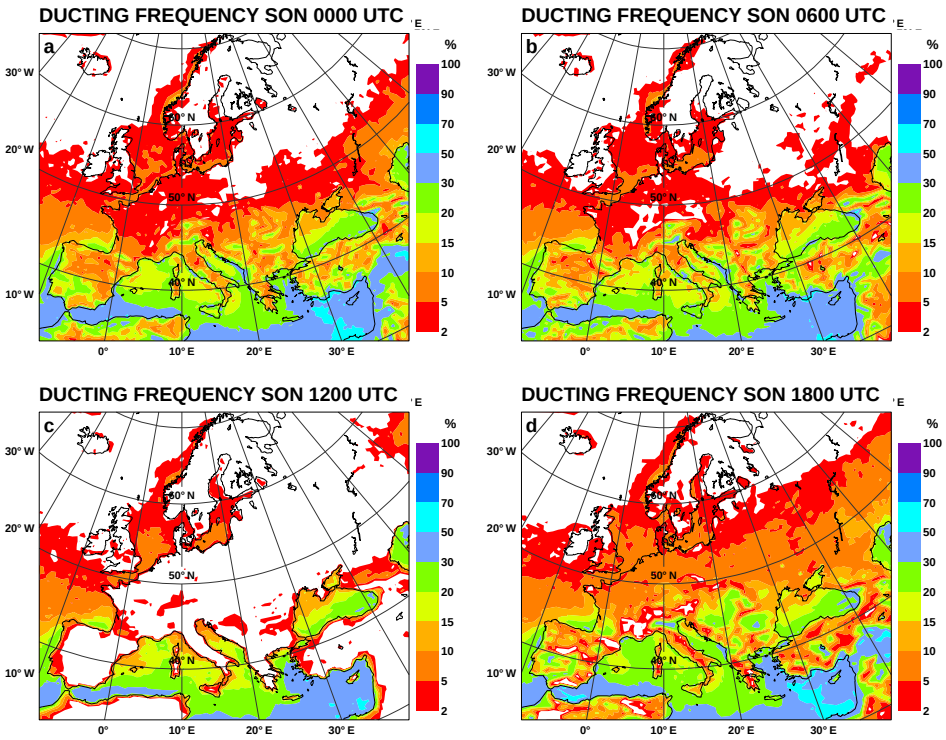

FIGURE 10: Same as in Fig. 7, but for autumn

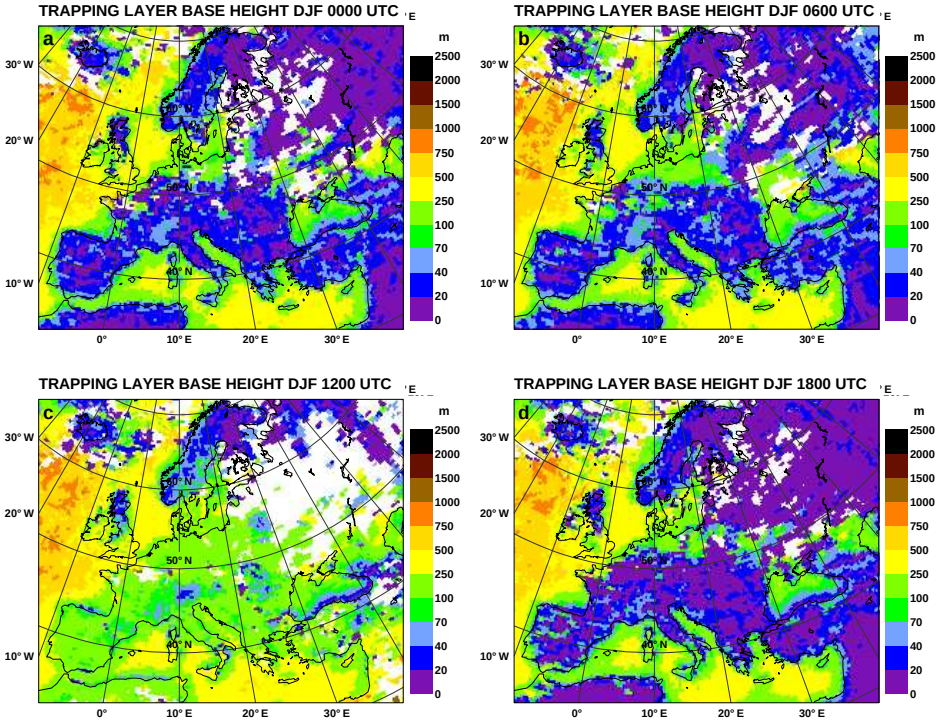

FIGURE 11: Mean winter trapping layer base height (m) over Europe at (a) 0000, (b) 0600, (c) 1200 and (d) 1800 UTC. White shading corresponds to duct-free regions.

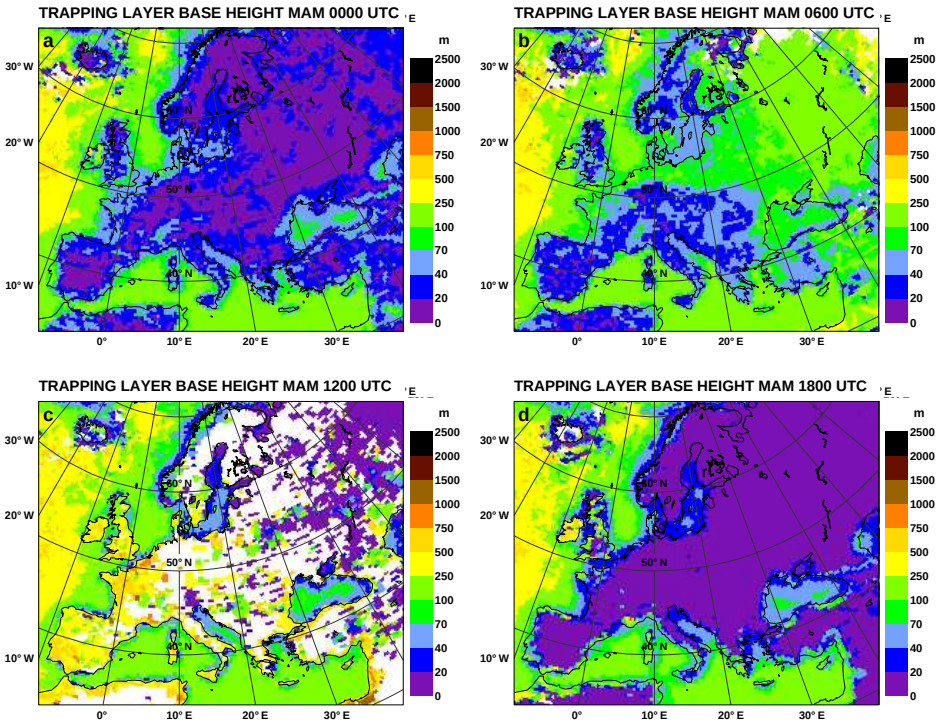

FIGURE 12: Same as in Fig. 11, but for spring.

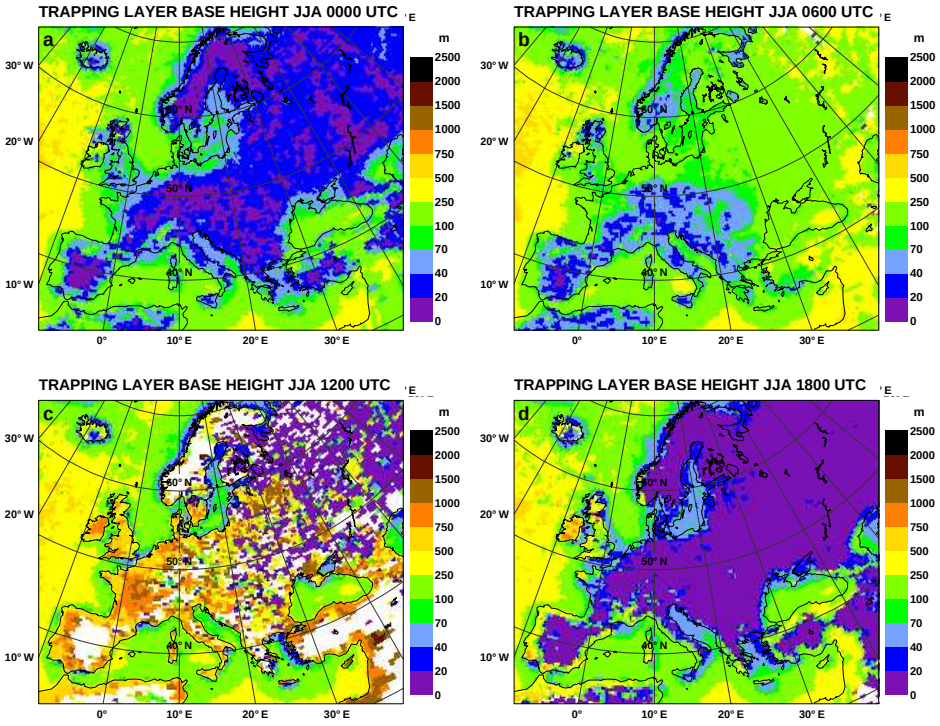

FIGURE 13: Same as in Fig. 11, but for summer.

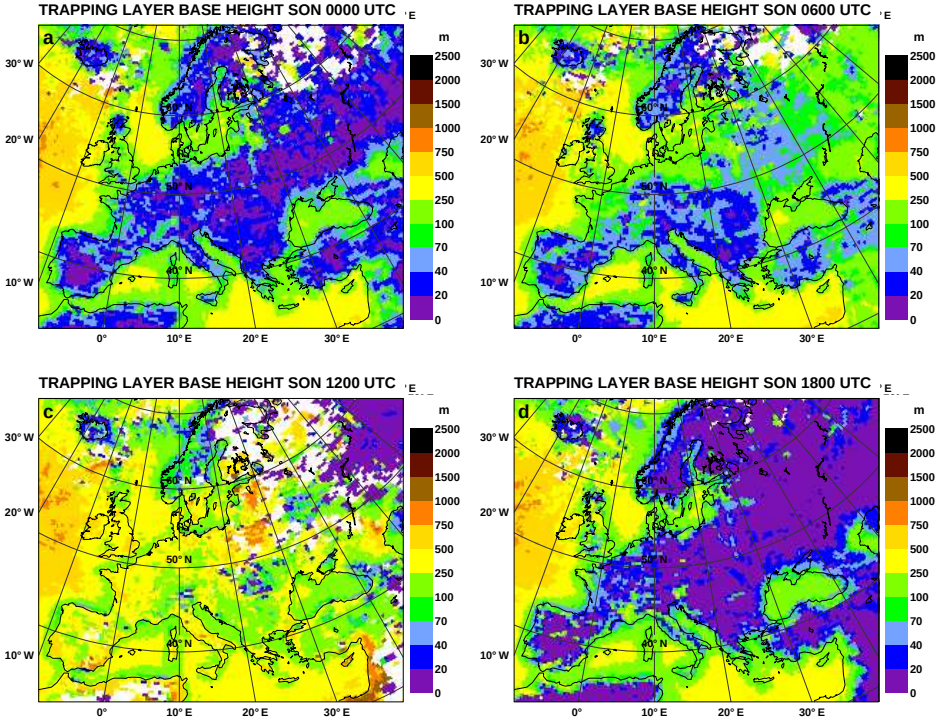

FIGURE 14: Same as in Fig. 11, but for autumn.

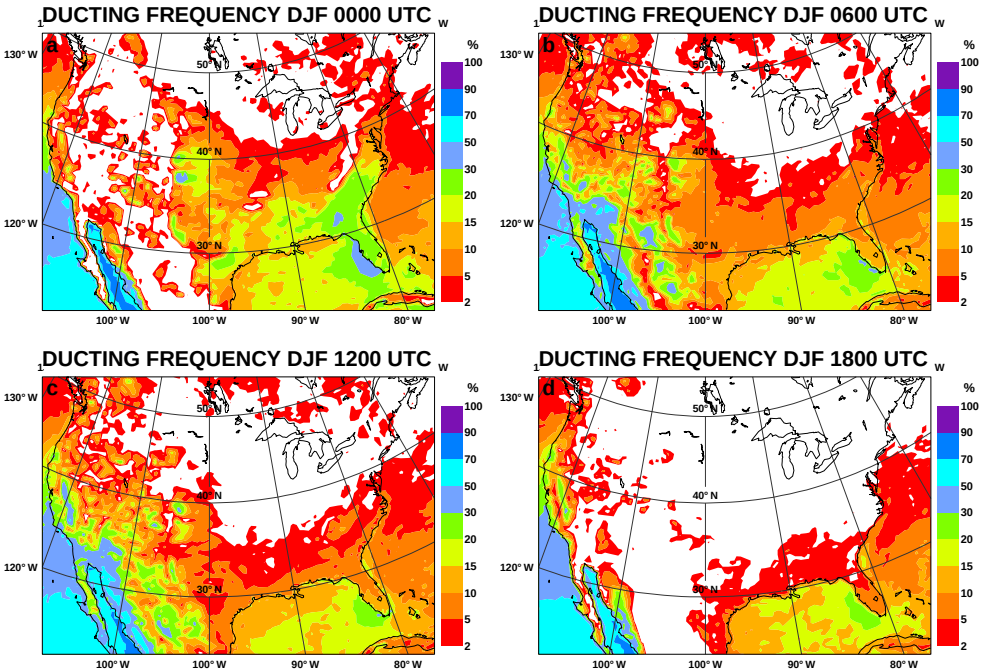

FIGURE 15: Mean winter frequency (%) of ducting conditions over the U.S.A. at (a) 0000, (b) 0600, (c) 1200 and (d) 1800 UTC.

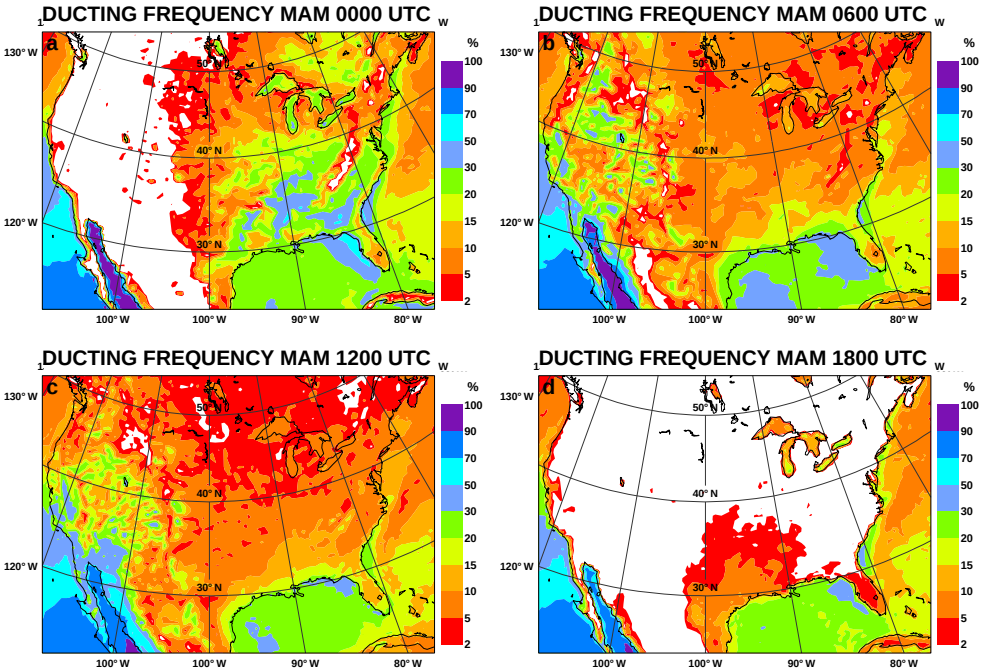

FIGURE 16: Same as in Fig. 15, but for spring.

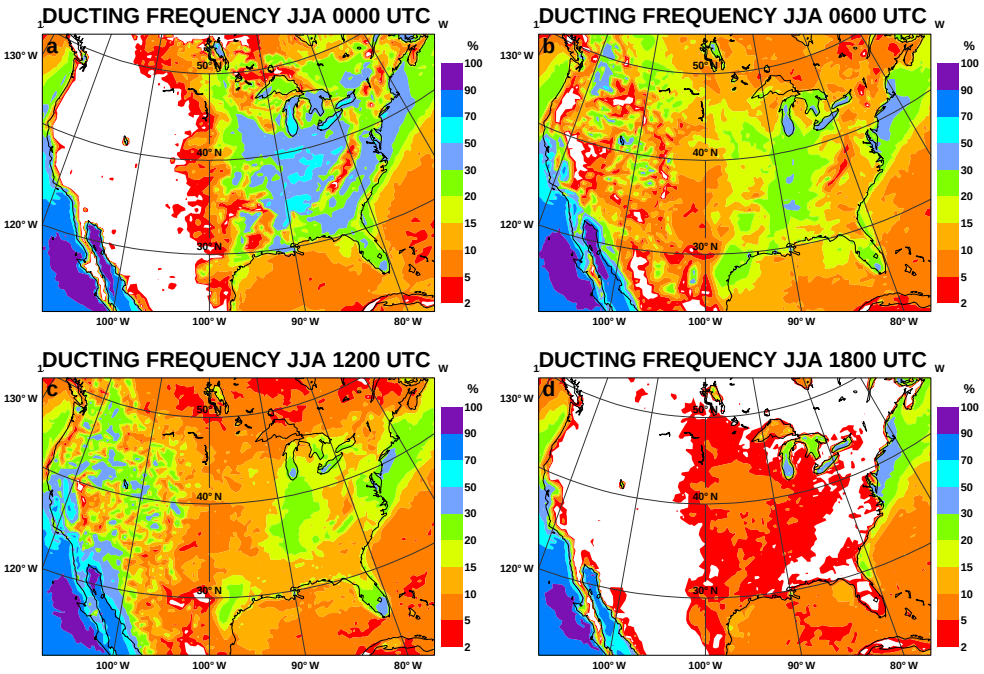

FIGURE 17: Same as in Fig. 15, but for summer.

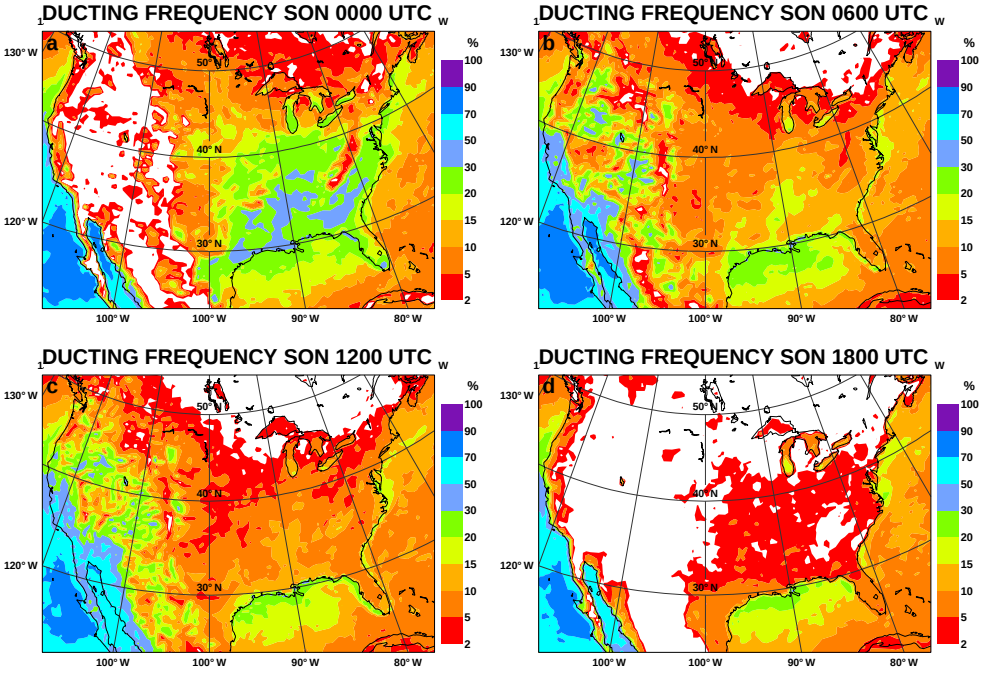

FIGURE 18: Same as in Fig. 15, but for autumn

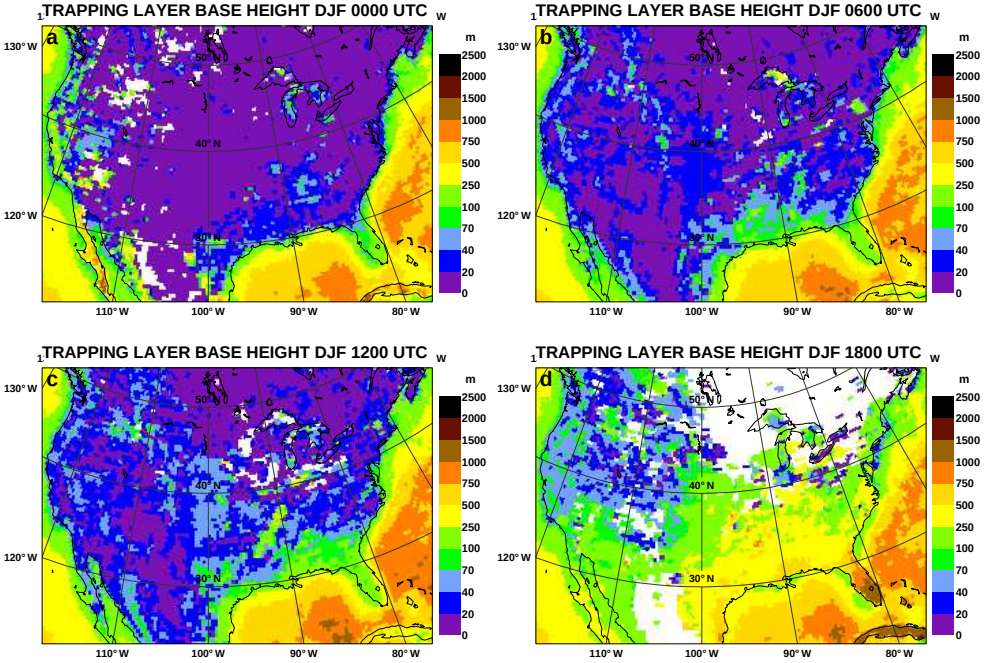

FIGURE 19: Mean winter trapping layer base height (m) over the U.S.A. at (a) 0000, (b) 0600, (c) 1200 and (d) 1800 UTC. White shading corresponds to duct-free regions.

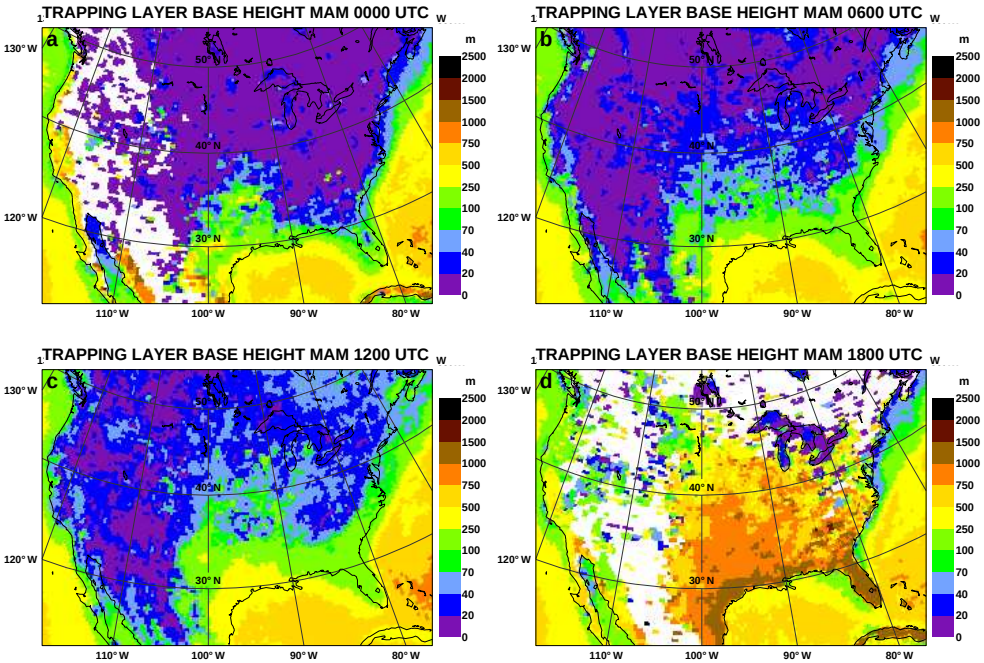

FIGURE 20: Same as in Fig. 19, but for spring.

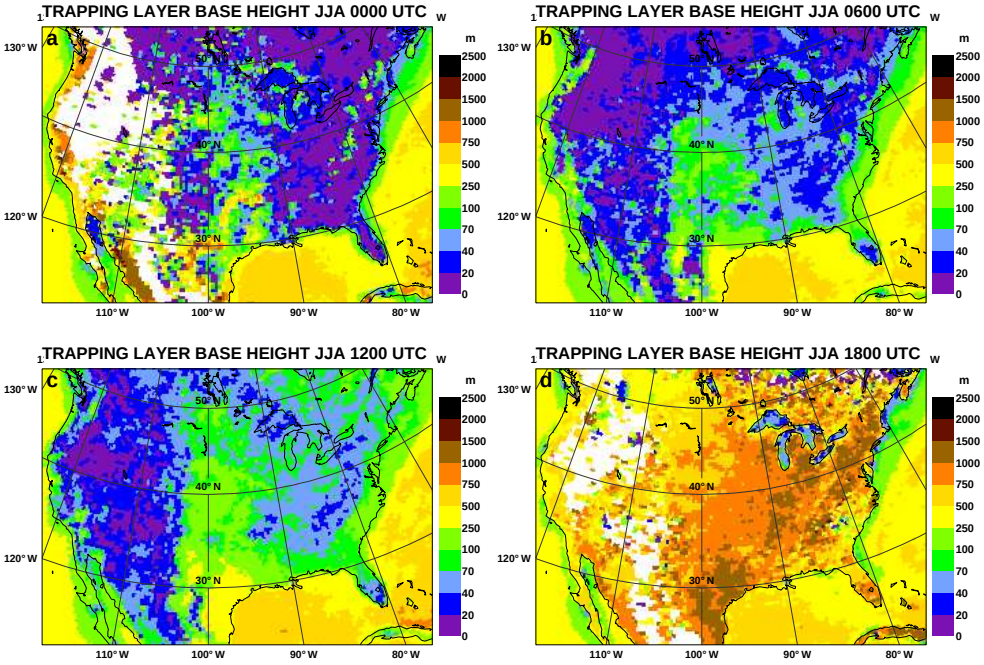

FIGURE 21: Same as in Fig. 19, but for summer.

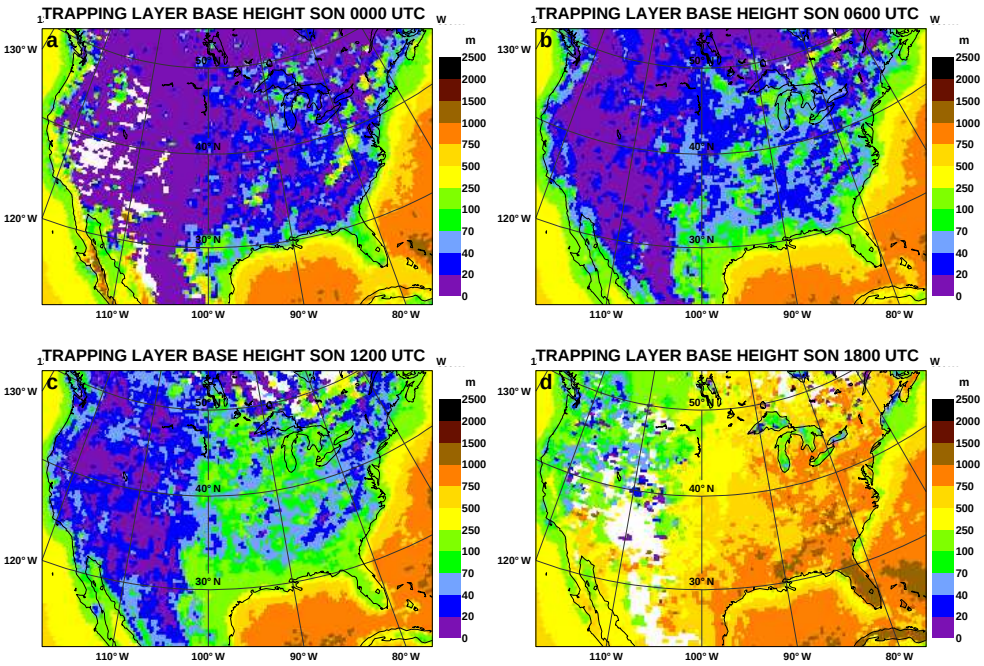

FIGURE 22: Same as in Fig. 19, but for autumn.

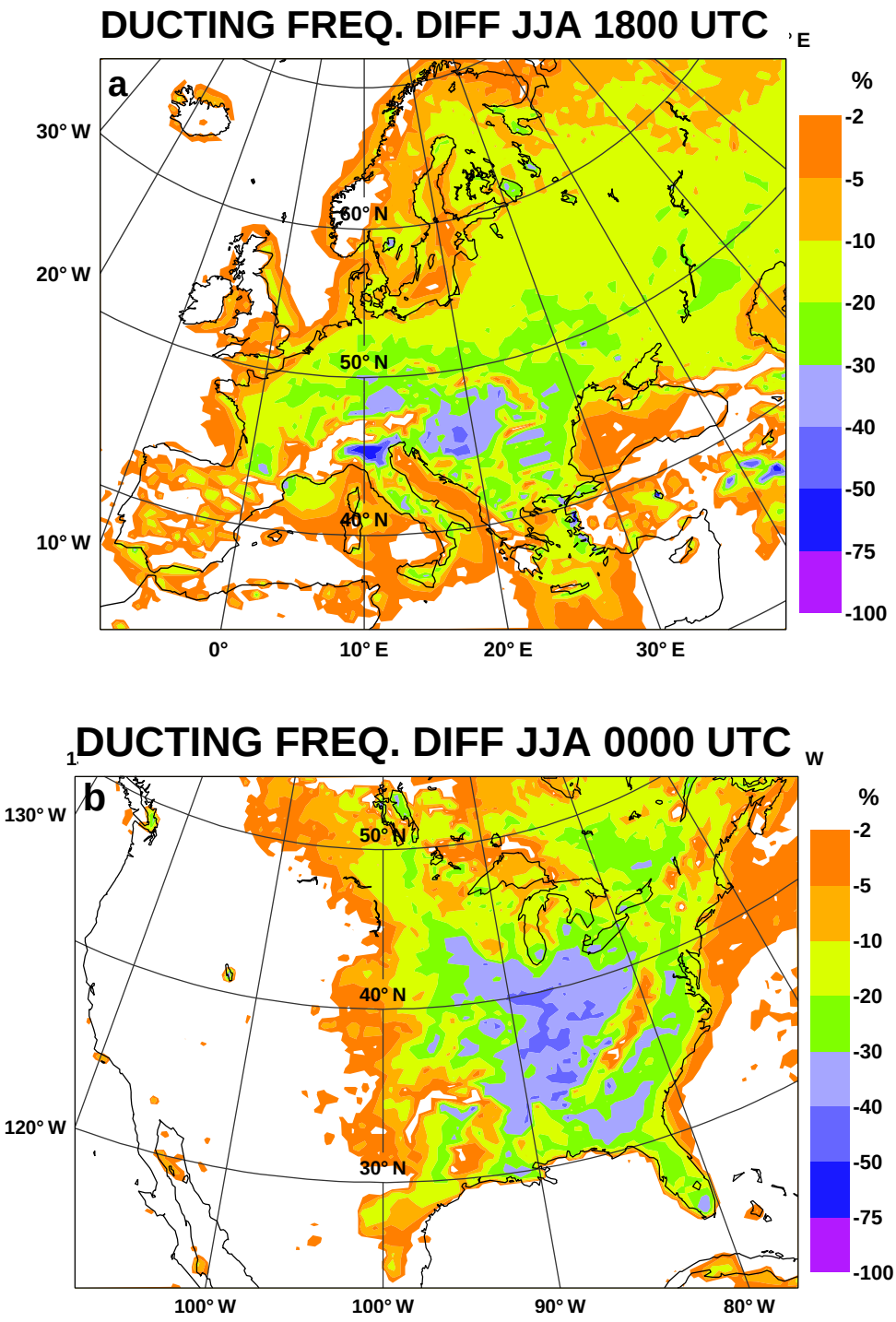

FIGURE 23: Mean CLIM35−CLIM10 summer difference in ducting frequency (%) (a) over Europe at 1800 UTC and (b) over the U.S.A. at 0000 UTC when refractivity gradient computations are started from the second lowest instead of the lowest model level.